Synthesis of N-doped Activated Carbon with Ultra-microporous and the Capacity to Store Hydrogen

Ze Liu,[a] Ye Xing,[a] Yande Cao,[a,b] and Haichao Li [a],*

N-doped ultra-microporous activated carbon was made from *Chenopodium quinoa* Willd. straw in the Tibetan Plateau region and cesium chloride as activator and used for H_2 adsorption and storage. Its structure was characterized by the Brunauer-Emmett-Teller (BET) method and other techniques. The results showed that the adsorbent had a well-developed microporous structure, and its specific surface area was as high as 804 $m^2 \cdot g^{-1}$. Its major pore sizes were all distributed in the ultra-micropores of 0.62 nm. The adsorbent also had a high H_2 adsorption storage capacity, which could reach 12.2 $cm^3 \cdot g^{-1}$ at an adsorption pressure of 1 MPa and an adsorption temperature of 298 K. This study provides a new way to improve the high value utilization of *Chenopodium quinoa* Willd. straw and solid hydrogen storage and provides corresponding evidence that CsCl can be used as an activator for ultra-microporous activated carbon.

DOI: 10.15376/biores.20.1.672-682

Keywords: Ultra-microporous; Activated carbon; Hydrogen; Adsorption storage; Chenopodium quinoa Willd.

*Contact information: a: Key Laboratory of Applied Physical Chemistry of Qinghai Province, Qinghai Minzu University, Xining 810007, Qinghai, China; b: Asia Silicon (Qinghai) Co., Ltd, Xining 810007, China; *Corresponding author: lihaichao@vip.163.com*

INTRODUCTION

Hydrogen energy is a new type of environmentally friendly and renewable energy, which is of great significance in alleviating the depletion of fossil energy. In recent years, with the deepening of the research on hydrogen storage materials, hydrogen storage materials have been widely used, such as in vehicles, fuel cells, and ships (Ren *et al*. 2017). However, hydrogen is a chemically active gas, resulting in stringent storage and transportation requirements. As a result, the existing methods of hydrogen storage present challenges regarding safety and economic efficiency (Ayvaz *et al*. 2018). Currently, popular hydrogen storage materials include metal complex hydride hydrogen storage materials, solid state hydrogen storage materials, and organic liquid hydrogen storage materials, all of which have advantages and disadvantages. For instance, metal complex hydride hydrogen storage materials have low storage pressure but poor cyclic stability (Michael *et al.* 2009). Solid-state hydrogen storage materials are safe, do not require high pressure, and are easy to transport, but the release conditions are harsh (Kumar *et al*. 2022). Organic liquid hydrogen storage materials have high hydrogen storage density, high safety, convenient storage and transportation, but expensive cost and harsh reaction conditions limit their development (Rao *et al*. 2023). In summary, it is necessary to develop a new type of hydrogen storage material that can overcome these deficiencies.

Chenopodium quinoa Willd. (quinoa) is native to the mid to high altitude mountains of the Andes in South America. Now it has become a favored crop in China's high-altitude plateau areas. Quinoa is mainly grown in Qinghai Province, Gansu Province, and Tibet, *etc*. Because of its high cold tolerance, high yield, and short growth cycle, it has become one of the few specialty crops that can be grown in the plateau area. It is also the signature crop of the Highlands region throughout the year (Wang *et al*. 2022; Tang *et al*. 2024). Due to the specific characteristics of quinoa straw (QS), it is not well suited as a source of direct feed for livestock. Also, leaving it in the field can interfere with farming the following year. In the past, burning was used, but this can pollute the environment (Zhao *et al*. 2020). It is also a serious waste of resources. Like most plant straws, QS's main components are lignin, cellulose, and hemicellulose. Previous studies have shown that the straw can be used as a source for the preparation of activated carbon after activation (Abril *et al*. 2022). Activators are usually zinc chloride ($ZnCl_2$), phosphoric acid (H_3PO_4), or potassium hydroxide (KOH). Currently, most of the activators are not recyclable, need to be adjusted to a pH-neutral value after activation, and even produce toxic gases (Zhang *et al*. 2024). The selection of activators limits the development of activated carbon materials. Interestingly, among the alkali metal elements with activating effects are Li, Rb, and Cs. Thus, CsCl can be used as an activator for cellulose-based activated carbon. Here, we activated quinoa straw by CsCl. Once again, the present work confirmed that CsCl has an activating effect (Yang *et al*. 2023; Zhang *et al*. 2024a; Zhang *et al*. 2024b; Zhang *et al*. 2024c).

In this experiment, QS was used as a carbon source and cesium chloride (CsCl) as an activator. The activation of QS by the chemical activation method made it possible for the complete recovery of CsCl at the end of the experiment. This work resulted in green nitrogen-doped ultramicroporous activated carbon adsorbent materials. Their storage capacity for hydrogen was evaluated.

EXPERIMENTAL

Materials

QS was obtained from cultivated land in Haixi Prefecture, Qinghai Province (situated at 37°23′ N 97°22′ E). CsCl was purchased from Shanghai Aladdin Biochemical Science and Technology Co., Ltd. and were analytically pure, and the reagent was used directly without special treatment.

Preparation of Ultramicroporous N-doped Activated Carbon

QS removed from the plowed fields was washed to remove soil and dried in an oven for 12 h. After crushing in a pulverizer, it was passed through a 200-mesh sieve. Using the Pepponacci method, 10 g of QS powder and CsCl were mixed in a crucible in the ratios of 0.5:1, 1:1, and 2:1, respectively, and deionized water was added until it exceeded the QS powder. Due to the non-contact and non-reaction between the solids, CsCl was uniformly dispersed in QS powder, giving full effect to the activation. The crucible was placed in an oven at 70 °C until most of the moisture was removed from the QS mixture. After removal, the crucible was placed in a muffle furnace. The temperature was increased to 500, 600, and 700 °C at a rate of 10 °C/min in an air atmosphere. The carbonization products were obtained by holding the temperature for 1, 2, 3, or 4. The activated samples were then filtered, dried, and ground in a mortar for further study.

Characterization Methods

The microstructural features of QSAC were observed using a Gemini 500 scanning electron microscope from Zeiss, Germany. Secondary electrons (SE) were used during the image collection process. Diffraction spectra obtained using a Shimadzu XRD-7000 diffractometer were tested to characterize the microcrystalline structure of QSAC.

Raman detection can be used to obtain the degree of graphitization of carbon materials. The Raman spectrum of QSAC was obtained at an excitation wavelength of 532 nm on a Thermo Fisher Scientific DxR2XI device. N_2 adsorption/desorption isotherms for QSAC at 77 K were obtained using BELSORPmax from MicrotracBEL Japan, Inc. Specific surface area and micropore volume were based on the Brunauer-Emmett-Teller (BET) method. The pore size distribution was estimated by the Horvath-Kawazoe (HK) model. The adsorption and desorption of H_2 was carried out at 298 K.

For Fourier transform infrared spectroscopy, the QSAC powder was mixed with KBr powder and then pressed into discs, which were examined using a Thermo Fisher NICOLET IS20.USA device.

Surface functional groups were analyzed by X-ray photoelectron spectroscopy with the ESCALAB 250XI model from Thermo Fisher Scientific, USA. Each photoelectron spectral region was scanned several times to obtain a good signal ratio. The C1s peak was set to 284.6 eV and used as an internal standard for the other peaks. The iodine adsorption value was determined according to GB/T 12496.8 (2015).

RESULTS AND DISCUSSION

Optimal Activation Process Selection

The fixed activation temperature was 700 °C, and the activation Salt-QS ratio was 1:1. The effect of activation time (0 to 3 h) on the yield of QSAC and the adsorption performance of iodine value was investigated. As shown in Fig. 1(a), the iodine adsorption value of QSAC increased with the increase of activation time from 0 to 2 h. The yield (27.18%) and iodine adsorption value (1,047.21 mg g^{-1}) of QSAC at 2 h were greater than the values obtained at other activation times. At 3 h, the yield and iodine adsorption value were significantly reduced compared with that at 2 h. With increasing time and carbonization temperature, the pore structure collapsed and the specific surface area decreased, which in turn led to a significant decrease in iodine value adsorption. Therefore, 2.0 h was selected as the optimal time.

The fixed activation time was 2 h, and the activation Salt-QS ratio was 1:1. The effect of activation temperature (500 to 800 ℃) on the yield of QSAC and iodine adsorption value was investigated. In Fig. 1(b), the QSAC yield decreased from 34.7% to 17.3% with the increase of activation temperature. The iodine adsorption value increased continuously, and at 700 ℃ the iodine adsorption value (1040 mg g^{-1}). The iodine adsorption value decreased when the temperature reached 800 ℃, when the yield (17.3%) and iodine adsorption value (774 mg g^{-1}) were the lowest. Therefore, 700 ℃ was selected as the optimal temperature.

The activation temperature was fixed at 700 °C and the activation time was 2.0 h. To investigate the effect of activated Salt-QS ratio on QSAC yield as well as iodine adsorption value. From Fig. 1(c), at a Salt-QS ratio of 0.5:1 (20.35%), the QSAC yield was the lowest compared to 1:1 (27.09%) and 1:2 (33.46%). At Salt-QS ratio 2:1, there was no remarkable increase in QSAC yield and iodine adsorption values compared to 1:1. The

optimal Salt-QS ratio was chosen to be 1:1 from the economic point of view. In summary, an activation time of 2 h, temperature of 700 °C, and a Salt-QS ratio of 1:1 was chosen as the characterization samples in the following experiments.

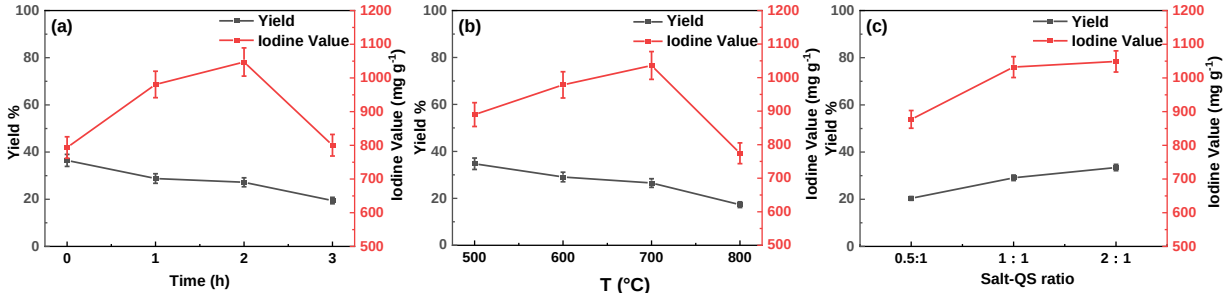

Fig. 1. Effect of activation parameters on QSAC yield and adsorption performance

Structural Characteristics

As shown in Fig. 2(a), without adding any activator, the surface of quinoa straw carbon (QSC) was rough, and the plant tissues were severely damaged. As shown in Fig. 2(b), when CsCl was added as an activator, the vascular bundles and basic tissues of QS activated carbon were more intact, with smooth surfaces and fewer pores, and most of the vascular bundles were hardly broken and collapsed. Compared to QSC, the surface of quinoa straw activated carbon (QSAC) maintains the basic characteristics of the plant's microstructure. The surface of QSAC was smooth and became more microporous, providing the materials with a larger specific surface area as well as better hydrogen adsorption capacity compared to QSC. This may be due to the addition of CsCl as an activator, which acts as a flame retardant and slows down the release of gaseous small molecules such as aromatic hydrocarbons, allowing the microstructure of the plant to be preserved. At the same time, during the gradual increase in temperature, small molecules such as aromatic hydrocarbons are slowly released, creating a large number of ultra-micropores (Hao *et al*. 2024). It is notable that micropores cannot be seen in such micrographs, since those pores are below the resolution of even the best electron microscopes.

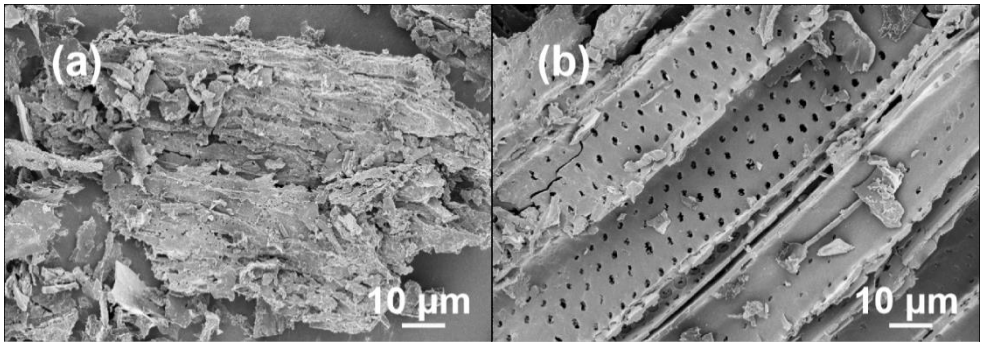

Fig. 2. SEM image of the samples. (a) QSC at 700 °C; (b) QSAC700

As shown in Fig. 3(a), the AC adsorption-desorption isotherm conformed to type I according to the IUPAC New Code-2015 Physical Adsorption Isotherm Classification method. The activated carbon had a very high adsorption value of N_2, as high as 239 cm^3 (STP) g^{-1} (Lee *et al*. 2016). The adsorption isotherm had a larger slope in the low relative

pressure region, especially in the low-pressure part (P/P_0 < 0.01) of the adsorption. N_2 adsorption tends to equilibrate with increasing relative pressure. This is mainly due to stronger interactions, indicating that QSAC is dominated by micropores. According to the BET method, the total pore volume of QSAC700 was 0.37 cm^3 g^{-1}, with an average pore size distribution of 1.82 nm, an overall distribution concentrated in the range of 0.46 to 0.86 nm, and a specific surface area of 804 m^2 g^{-1}. The results of the nitrogen adsorption-desorption curves are further corroborated from the pore size distribution plot in Fig. 3(b). The QSAC700 dominant pore size distribution is at 0.62 nm. According to the IUPAC New Specification-2015 Code, it can be determined that QSAC700 is a new type of ultra-microporous carbon material.

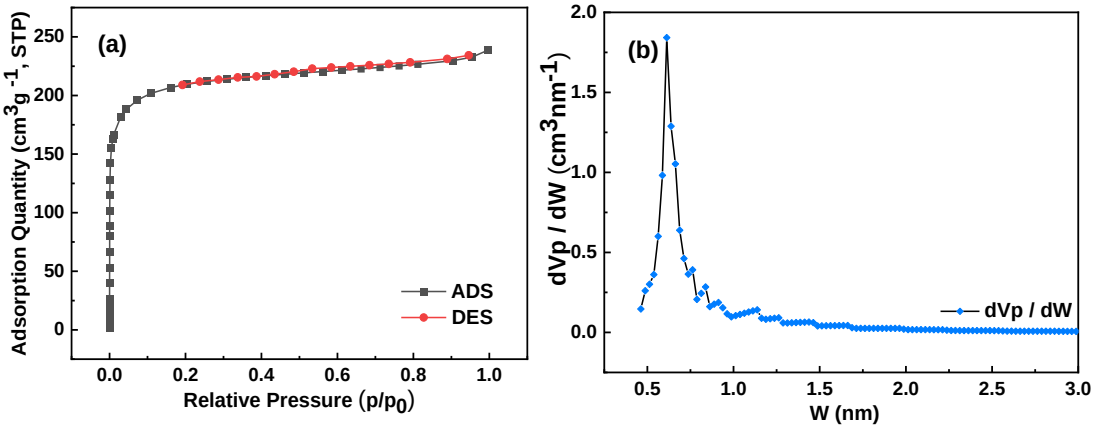

Fig. 3. (a) N_2 adsorption-desorption isotherms, (b) Pore size distribution of QSAC700.

The structural orderliness of QSAC700 was analyzed by XRD, as shown in Fig. 4(a). QSAC700 has a distinct characteristic diffraction spectrum of carbon. The (002) crystal plane and the (100) crystal plane have typical carbon characteristics at 2θ of about 26° and 43°. The d002 graphite layer spacing was calculated to be 0.372 nm by Bragg's formula, which is larger than the layer spacing of fully non-graphitized carbon (0.344 nm). It can be demonstrated that the prepared hollow carbon nanospheres were in the amorphous carbon stage, which can be graphitized by increasing the temperature.

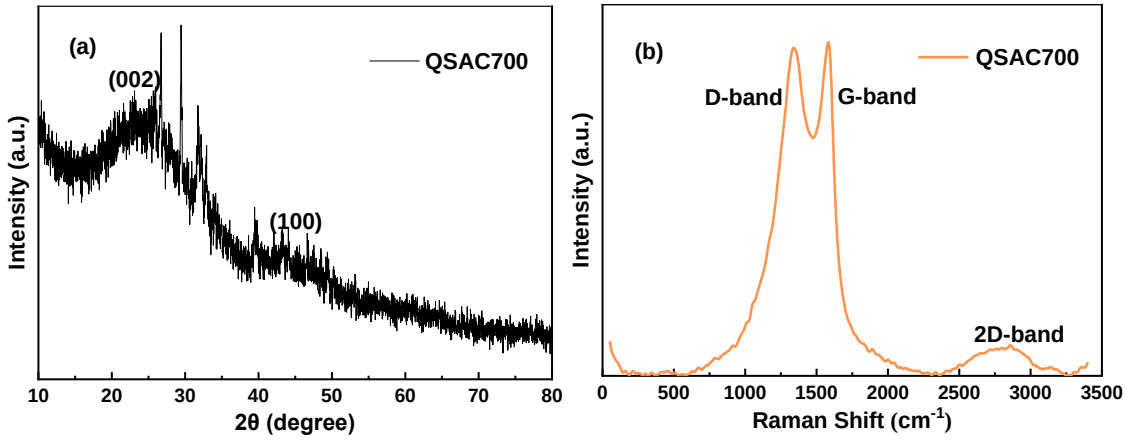

Fig. 4. (a) XRD spectra and (b) Raman spectra of QSAC700

As shown in Fig. 4(b), the presence of distinct D, G, and 2D bands in QSAC700 is typical of amorphous carbon. The intensity ratio of the D and G bands (I_D/I_G) has long been considered a key parameter for analyzing graphitization levels (Guo *et al*. 2021). The calculated I_D/I_G ratio of AC700 is 0.9834, which indicates that the prepared QSAC possessed some degree of graphitization (Zhou *et al*. 2016). This indicates that the interior of QSAC is transforming from a graphite disordered layer structure to an ordered one, and the microcrystalline defects are being gradually reduced. The slightly bulged 2D band near 2700 cm^{-1} also confirms that there were still some defects in the graphite layered structure.

As shown in Fig. 5, the characteristic peak shapes of QSC and QSAC infrared spectra were almost identical. The peaks around wave number 3,409 cm^{-1} are attributed to the O-H and O-N stretching vibrations. The peak at 2,525 cm^{-1} represented methylene stretching. The peak at 1,589 cm^{-1} is caused by the stretching vibration of the C=C bond of the benzene ring. The peak at 1,429 cm^{-1} is associated with the C-N stretching vibrational mode. The peaks at 1,032 cm^{-1} are those of C-O-C, C-O stretching vibrations and O-H bending vibrations in carboxylates, phenols, or alcohols. The peak at 871 cm^{-1} is an out-of-plane deformation vibrational peak of the aromatic ring. The 563 cm^{-1} peak is a bending vibration in the C-C=O plane. It can be seen that the main structure of activated carbon consists of multiple aromatic rings. The aromatic ring may also have functional groups such as $-CH_3$, $-CH_2$, -COOH, and -OH. The absorbance peaks of QSAC at 3,409 cm^{-1} and 1,032 cm^{-1} were significantly broader than those of QSC, suggesting that the activated carbon may contain more oxygen-containing functional groups dominated by C-O and O-N bonds. This is due to the increase in the content of highly substituted aromatic rings as a result of the polycondensation of QS by the carbonization process. Addition of CsCl activator reduces the breakage of chemical bonds connecting the carbon network. It indicates that the prepared QSAC contains sufficient carbon framework and abundant organic functional groups, which in turn makes the activated carbon exhibit strong adsorption properties (Gao *et al*. 2013).

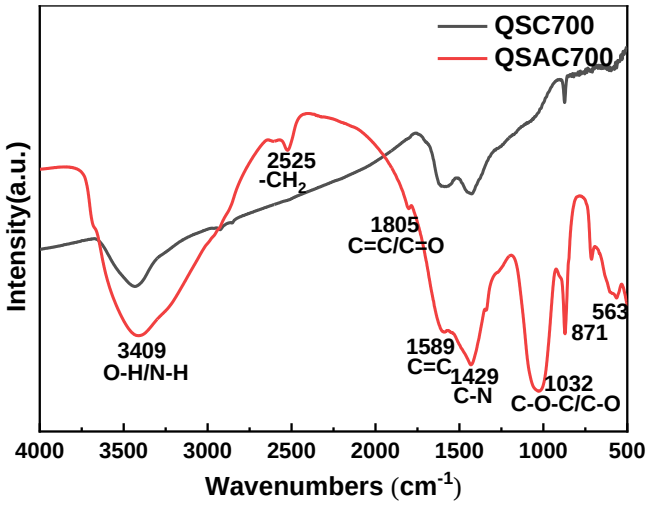

Fig. 5. FT-IR spectra of QSC700 and QSAC700

X-ray photoelectron spectroscopy is commonly used to characterize the chemical structure of material surfaces. Figure 6 shows that QSAC700 contained C, N, and O elements. From Figs. 6 (b) to 6 (d), the C1s spectrum splits into three peaks. It is shown

that there are five possible bonding forms of C, namely C=C (284.8 eV), C-O/C=N (286.7 eV) and C-O/C-N (288.8 ev). O1s split into 2 peaks, C-O (533.5 eV), and C=O (531.6 eV). N1s then splits into 2 peaks, pyridine N (399.1 ev) and graphitized N (400.4 eV). Both XPS and FTIR data indicated the presence of O and N in the sample, suggesting that the prepared QSAC700 is N-doped amorphous carbon (Du *et al*. 2024).

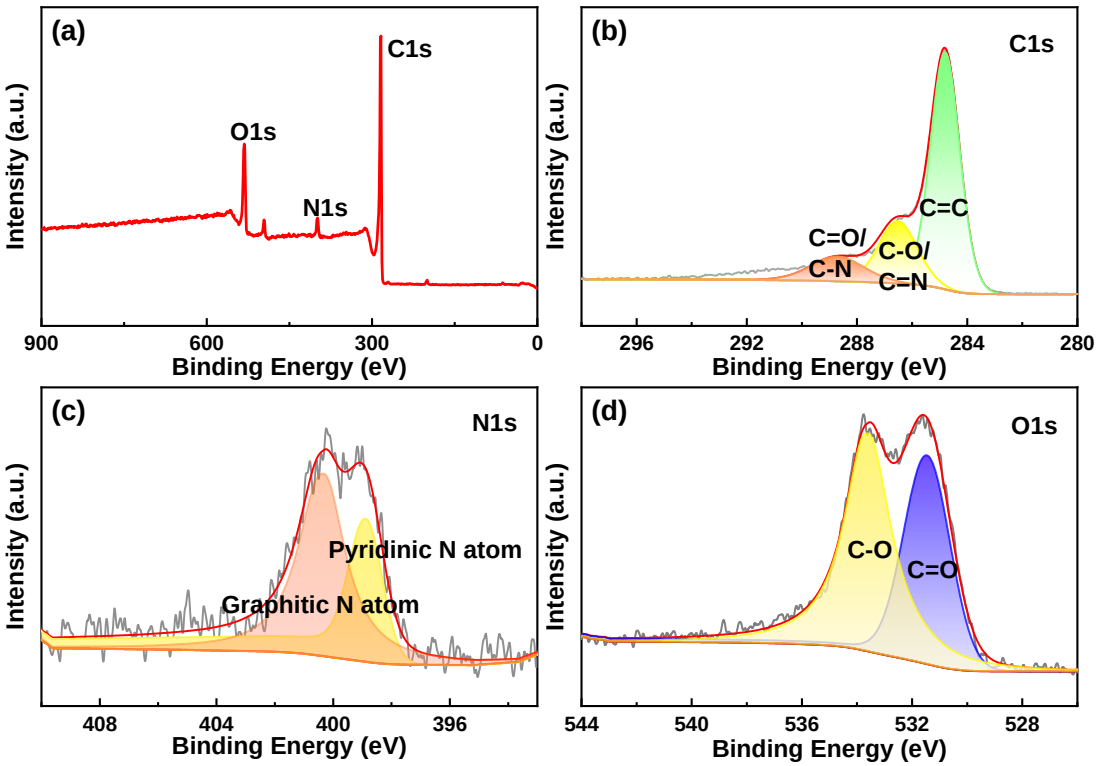

Fig. 6. XPS survey (a) and fitted spectra of C1s (b), O1s (c) and N1s (d) of QSAC700

Theoretical calculations and experiments have shown that the physical adsorption of hydrogen on nanomaterials under low-temperature liquid nitrogen conditions depends on the microporous volume and microporous size distribution, especially the microporous volume size is closely related (Zhao *et al*. 2012). This is due to the fact that hydrogen molecules are smaller, so their adsorption efficiency is higher on micropores than on mesopores. In general, there was a good linear relationship between hydrogen storage and microporous pore volume, *i.e*., the larger the microporous pore volume, the larger the hydrogen storage. Schaefer demonstrated that pores with widths ranging from 0.5 to 0.7 nm are best suited for hydrogen storage at 298 K, independent of pressure (Schaefer *et al*. 2016). Based on this, it is hypothesized that QSAC700 should be a good material for hydrogen storage. The atmospheric pressure hydrogen adsorption and desorption curves for QSAC700 under cryogenic liquid nitrogen conditions are shown in Fig. 7. As can be seen from the results in Fig. 7, the adsorption capacity of hydrogen reached 35 cm^3 g^{-1} at 298 K and 101.3 KPa, which is higher than the 0.59 wt% reported in literature (Schaefer *et al*. 2016). It was shown that the AC700 microporous structure had excellent hydrogen storage capacity. It is also important to note that QSAC had excellent reversibility as a hydrogen storage material. As the pressure dropped, the physically adsorbed hydrogen could be completely and reversibly desorbed without hysteresis loops. With the same

specific surface area, the hydrogen storage capacity was higher than that of activated carbon based on rice husk (Kızılduman *et al*. 2021), sucrose (Krishnamurthy *et al*. 2014), bamboo and other raw materials (Jang *et al*. 2020), as shown in Table 1.

Table 1. Thermal Stability Parameters of Different Activated Carbons

References	Starting Materials	Hydrogen Storage Capacity (wt%)	Specific Surface Area ($cm^3\ g^{-1}$)
Kızılduman *et al*. (2021)	Rice husk	1.1	92
Krishnamurthy *et al*. (2021)	Sucrose	0.9	284
Jang *et al*. (2020)	Bamboo	1.35	559
In this study	Quinoa straw	1.1	803

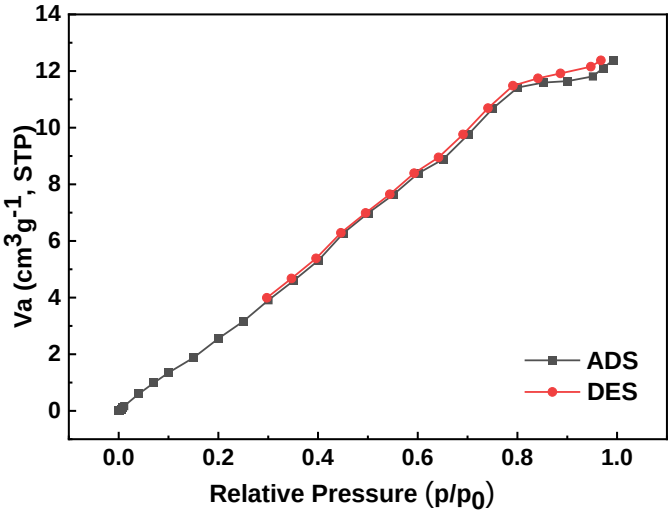

Fig. 7. Hydrogen storage capacity of QSAC700

CONCLUSIONS

1. This work was based on quinoa straw (QS) as a raw material, and CsCl was used as an activator at 700 °C. Nitrogen-doped ultramicroporous activated carbon (QSAC) was prepared by a one-step carbonization method. The optimal process for the preparation of QSAC was determined by the Pepponacci method as follows: activation temperature of 700 ℃, activation time of 2 h and Salt-QS ratio of 1:1.
2. The specific surface area of QSAC reached 804 $m^2 \cdot g^{-1}$ with a pore volume of 0.37 $cm^3 \cdot g^{-1}$ and a dominant pore size of 0.62 nm. Among the carbon materials with the same specific surface area biomass activated carbon, it had a higher percentage of micropores and higher surface nitrogen and oxygen heteroatom content.
3. The adsorption capacity of hydrogen reached 35 $cm^3 \cdot g^{-1}$ at room temperature and pressure, which has excellent hydrogen storage capacity.

4. It was demonstrated that CsCl could be used as a novel activator for the activation of QS for the preparation of N-doped ultramicroporous activated carbon. This approach provides a new way to solve the problem of agricultural waste occupying arable land and the diversified utilization of salt lake products.

ACKNOWLEDGMENTS

The authors are grateful for the support of the Key R&D and Transformation Program of Qinghai (2022-QY-210).

REFERENCES CITED

Abril, D., Ferrer, V., Mirabal, G. Y., Cabrera, B. G., Segura, C., Marican, A., Pereira, A., Durán-Lara, E. F., and Valdés, O. (2022). "Comparative study of three dyes' adsorption onto activated carbon from *Chenopodium quinoa* Willd and *Quillaja saponaria*," *Materials* 15(14), article 4898. DOI: 10.3390/ma15144898

Ayvaz, M., Ayvaz, S. İ., and Aydin, İ. (2018). "A novel method for determining effects of fire damage on the safety of the Type I pressure hydrogen storage tanks," *Int. J. Hydrog. Energy* 43(44), 20271-20283. DOI: 10.1016/j.ijhydene.2018.05.092

Du, B. X., Li, H. C., Zhang, C. L., and Ji, Q. S. (2024). "Construction of carbon nanospheres: A rational design based on BS-12 @ LiCl," *Heliyon* 10 (6), article e27585. DOI: 10.1016/j.heliyon.2024.e27585

Gao, Y., Yue, Q., Gao, B., Sun, Y., Wang, W., Li, Q., and Wang, Y. (2013). "Preparation of high surface area-activated carbon from lignin of papermaking black liquor by KOH activation for Ni(II) adsorption," *Chem. Eng. J.* 217 345-353. DOI: 10.1016/j.cej.2012.09.038

GB/T 12496.8 (2015). "Test methods of wooden activated carbon—Determination of iodine number," Standardization Administration of China, Beijing, China.

Guo, D., Fu, Y., Bu, F., Liang, H., Duan, L., Zhao, Z., Wang, C., ElToni, A. M., Li, W., and Zhao, D. (2021). "Monodisperse ultrahigh nitrogen-containing mesoporous carbon nanospheres from melamine-formaldehyde resin," *Small Methods* 5, article 2001137. DOI: 10.1002/smtd.202001137

Hao, S., Zhang, Q., Shi, Y., Guo, Q., Li, P., and Huang, J. (2024). "Preparation and characterization of the poplar micro-nano cellulose sustainable carbon spheres," *Biomass Conv. Bioref.* 14, 9581-9594. DOI: 10.1007/s13399-022-03003-0

Jang, H. S., Mun, J. Y., Hong, W. G., Lee, S. M., Jeon, J. W., Lee, C. Y., Kim, H. J., and Kim, B. H. (2020). "The performance of green carbon as a backbone for hydrogen storage materials," *Int. J. Hydrog. Energy*. 45 (17), 10516-10522. DOI: 10.1016/j.ijhydene.2019.03.084

Kızılduman, B. K., Turhan, Y., and Doğan, M. (2021). "Mesoporous carbon spheres produced by hydrothermal carbonization from rice husk: Optimization, characterization and hydrogen storage," *Adv. Powder Technol*. 32 (11), 4222-4234. DOI: 10.1016/j.apt.2021.09.025

Krishnamurthy, G., Namitha, R., Agarwal, S. (2014). "Synthesis of carbon nanotubes and carbon spheres and study of their hydrogen storage property by electrochemical method," *Procedia Mat. Sci*. 5, 1056-1065. DOI: 10.1016/j.mspro.2014.07.397

Kumar, A., Muthukumar, P., Sharma, P., and Kumar, E. A. (2022). "Absorption based solid state hydrogen storage system: A review," *Sustain Energy Technol. Assess*. 52 (c), article 102204. DOI: 10.1016/j.seta.2022.102204

Lee, S., Lee, M. E., Song, M. Y., Cho, S. Y., Yun, Y. S., and Jin, H. (2016). "Morphologies and surface properties of cellulose-based activated carbon nanoplates," *Carbon Letters* 20, 32-38. DOI: 10.5714/CL.2016.20.032

Michael, C. G., Eustathios, S. K., Sofoklis, S. M., Konstantinos, K., and Efstratios, N. P. (2009). "Design and optimization of advanced materials and processes for efficient hydrogen storage," *Comput. Chem. Eng*. 33 (5), 1077-1090. DOI: 10.1016/S1570-7946(09)70031-8

Rao, P. C., Kim, Y. S., Kim, H., Son, Y. H., Choi, Y. Y., Na, K., and Yoon, M. Y. (2023). "Methylbenzyl naphthalene: Liquid organic hydrogen carrier for facile hydrogen storage and release," *ACS Sustainable Chem. Eng.* 11 (34), 12656-12666. DOI: 10.1021/acssuschemeng.3c02689

Ren, J. W., Musyoka, N. M., Langmi, H. W., Mathe, M., and Liao, S. J. (2017). "Current research trends and perspectives on materials-based hydrogen storage solutions: A critical review," *Int. J. Hydrog. Energy* 42 (1), 289-311. DOI: 10.1016/j.ijhydene.2016.11.195

Schaefer, S., Fierro, V., Izquierdo, M. T., and Celzard, A. (2016). "Assessment of hydrogen storage in activated carbons produced from hydrothermally treated organic materials," *Int. J. Hydrog. Energy* 41(28), 12146-12156. DOI: 10.1016/j.ijhydene.2016.05.086

Tang, Y. M., Liu, Y. Z., Zhang, Y. H., Cao, Y. N., Song, P. P., Hou, L. M., and Peng, L. X. (2024). "A comparative analysis of the nutrient and phytochemical richness among different varieties of quinoa in China," *Food Sci. Nutr*. 1-13. DOI: 10.1002/fsn3.4113

Wang, N., Wang, F. X., Shock, C., Fritschi, F. B., Gao, L., Huang, Z. J., and Zhao, J. Y. (2022). "Optimizing quinoa height to counter stem lodging risks in the three main production regions of China," *Agric. For Meteorol*. 323, article 109084. DOI: 10.1016/j.agrformet.2022.109084

Yang, J. Y., Zhang, X. P., and Li, H. C. (2023). "Preparation of activated carbon by lithium chloride activation and its performance for lithium ion adsorption," *Chemistry* 86(11), 1383-1388+1382. DOI:10.14159/j.cnki.0441-3776.2023.11.006

Zhang, C. L., Li, H. C., Lin, Z. Z., Du, B. X., and Zhang X. P. (2024a). "Preparation and characterization of polyvinyl chloride based carbon materials with high specific surface area," *Carbon Trends* 14, article 100322. DOI: 10.1016/j.cartre.2024.100322

Zhang, C. L., Li, H. C., and Du, B. X. (2024b). "Preparation and characterization of cellulose-based activated carbon by cesium chloride chemical method," *BioResources* 19(1), 1295-1304. DOl: 10.15376/biores.19.1.1295-1304

Zhang, C. L., Li, H. C., and Du, B. X. (2024c). "Preparation and characterization of lignin-based activated carbon by rubidium chloride chemical method," *ChemistrySelect* 9(20), article e202401258. DOl: 10.1002/slct.202401258

Zhao, W., Fierro, V., Fera'ndez-huerta, N., Izquierdo, M. T., and Celzard, A. (2012). "Impact of synthesis conditions of KOH activated carbons on their hydrogen storage capacities," *Int. J. Hydrog. Energy* 37(19), 14278-14284. DOI: 10.1016/j.ijhydene.2012.06.110

Zhao, X. L., Wang, F., Fang, Y., Zhou, D. W., Wang, S. P., Wu, D. Q., Wang, L. X., and Zhong, R. Z. (2020). "High-potency white-rot fungal strains and duration of fermentation to optimize corn straw as ruminant feed," *Bioresource Technology* 312, article 123512. DOI: 10.1016/j.biortech.2020.123512

Zhou, C., Geng, S., Xu, X. W., Wang, T. H., Zhang, L. Q., Tian, X. J., Yang, F., Yang, H. T., and Li, Y. F. (2016). "Lightweight hollow carbon nanospheres with tunable sizes towards enhancement in microwave absorption," *Carbon* 108 234-241. DOI: 10.1016/j.carbon.2016.07.015

Article submitted: September 25, 2024; Peer review completed: October 19, 2024;
Revisions accepted: November 12, 2024; Published: November 20, 2024.
DOI: 10.15376/biores.20.1.672-682